ESO-TP-73J
Jan 1997

DEC 23 1997

LIBRARY

Stellar Surface Observations with the VLTI

O. von der Lühe

European Southern Observatory
Karl-Schwarzschild-Str. 2, D - 85748 Garching

ESO-TP-73J

Abstract. The resolution of the VLTI approaches 0.5 milli-arcsec at visible wavelengths and 1 milli-arcsec in the near infra-red. This is sufficient to resolve about 2000 near-by bright stars. The surface of about 400 stars, mainly K and M giants, can be mapped with a resolution of a dozen pixels or better across the stellar surface. This resolution permits detailed studies of the structure of stellar atmospheres, their hydrodynamics and magneto-hydrodynamics. VLTI can easily resolve starspots and very likely also convection cells on an active K-type giant at 10pc distance. A marginal detection of the largest starspots on a very active solar-type star at the same distance may be possible, but it appears very unlikely that the surface structure on an inactive solar-type star can be imaged.

Computer simulations of stellar surfaces were used to study in detail the response of the VLT interferometer to an extended, complex source. First results which simulate the end-to-end process in a simplified manner indicate that useful maps can be produced provided that a sufficient number of baselines are combined in Earth-rotation synthesis mode. We investigate the signal to noise ratio which which one could expect to observe stellar surface structure and conclude that the VLTI will provide sufficient sensitivity.

1 Introduction

Stars will be one of the major science targets of the VLTI. The surface of many near–by stars can be mapped with a resolution of better than a dozen pixels across the stellar surface. High angular resolution permits detailed studies of the structure of stellar atmospheres, their hydrodynamics and magneto-hydrodynamics. Although potential target stars are usually bright, the large collecting area of VLTI is essential for measuring the faint fringes resulting from the resolved stellar surface at spectral resolution high enough to resolve spectral line features. In order to better understand the requirements, we are in the process of developing detailed models of stellar surfaces to simulate observations with VLTI. We have already presented some science goals and results in two earlier papers (von der Lühe et al. 1995, von der Lühe et al. 1996). Some of these results are reproduced here. In addition, we present detailed analyses of the expected sensitivity of the VLTI. It is shown that stars with apparent diameters which can be resolved by the VLTI are also bright enough for on-source fringe tracking at shorter baselines, allowing to integrate the faint fringe signal at longer baselines with high sensitivity at high spectral resolution.

Fermilab Library
0 1160 0064845 5

2 Statistics

The apparent diameter of a star must at least be of the order of the narrowest fringe spacing to be resolved by an interferometer. The VLTI with its baselines of about 100 m will be capable to resolve 0.5 milli-arcsec at visible wavelengths and about 1 milli-arcsec at 1 μm. This will suffice to derive a few fundamental parameters of stellar structure, such as diameters and center-to-limb variation as a function of the wavelength, for stars with diameters of the order of the milli-arcsec. Detailed surface structure will be observable for stars with diameters of about 5 milli-arcsec and bigger. The *Catalogue of Apparent Diameters and Absolute Radii of Stars* (CADARS; Fracassini et al. Fracassini, et al., 1988) was used to investigate the potential of VLTI for resolving stellar surfaces. The catalogue data should be within a factor of two or three from the truth, sufficient to assess the order of magnitude of potential targets for VLTI.

Fig. 1 presents a histogram of the diameter distribution of all sources in the catalogue with an apparent diameter larger than a milli-arcsec and a declination of less than 40 degrees, which is within reach from Cerro Paranal with VLTI baselines. There is a total of 1309 such sources. The figure shows cumulative histograms for different spectral types, as well as the overall cumulative distribution. Virtually all stars which are potentially resolved by VLTI are late types, in particular K Giants. About 50% of all stars shown have apparent diameters of less than 2.5 milli-arcsec; little more than just estimating diameters and CLVs will be possible for those. About 20% or some 260 are larger than 5 milli-arcsec. It should be possible to produce fairly detailed maps, with a resolution of at least 5 by 5 pixels. Only 7% or some 90 stars, and all of them K and M stars, are larger than 10 milli-arcsec, and are already resolved by the VLT Unit telescopes at visible wavelengths. Detailed surface maps will be possible for those stars provided that good baseline coverage is achieved. VLTI has a particular edge here, because there are four big telescopes which can be combined with relocatable auxiliary telescopes.

Fig. 2 shows a scatter diagram of the angular diameters vs. visual magnitude of the selected CADARS sources. The catalogue is evidently not complete since stars with $m_V > 6.5$ and apparent diameters of less than 5 milli-arcsec are underrepresented. The main conclusion here is that resolved stars are bright. There are no stars with visual magnitudes fainter than 12 in the sample, the bulk has magnitudes between 2 and 7. These sources can therefore serve as their own reference sources for adaptive optics which will perform near the diffraction limit at near infrared – and at later stages of the observatory's development also visible – wavelengths. This circumstance makes VLTI very sensitive for measuring low visibilities. Because of the bias towards brighter stars one can expect many more stars, about a factor 0.5 to 1 of the present sample, at magnitudes above 6.5 and with apparent diameters less than 10 milli-arcsec. These will be predominantly K and M stars. In total, one can expect about 2000 stars to be resolved with VLTI, out of which some 400 will be large enough to obtain maps of surface detail.

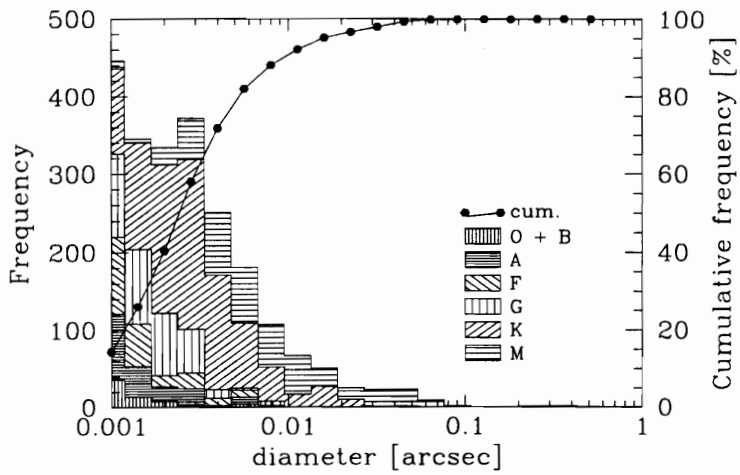

Fig. 1. Histogram of CADARS stars with apparent diameters larger than 0.001 arcsec and declinations below 40 degrees.

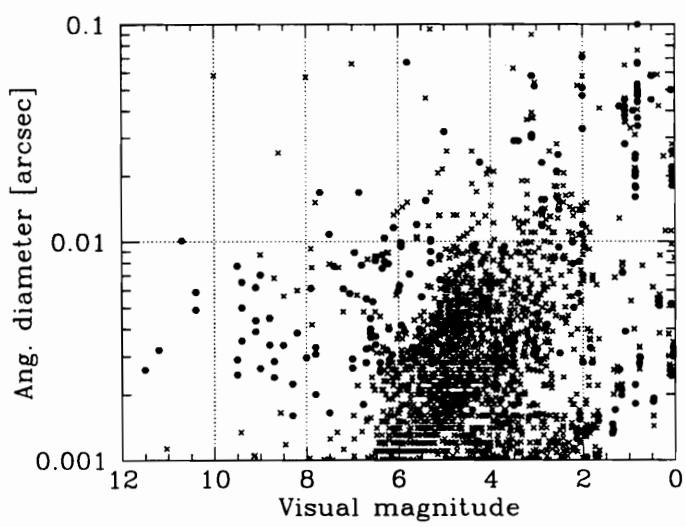

Fig. 2. Apparent angular diameters vs. visual magnitude of CADARS stars with declinations below 40 degrees. Solid dots: direct techniques, crosses: indirect techniques.

3 Stellar Surface Phenomena and Visibility Functions

The range of surface phenomena on stars has been discussed in depth in von der Lühe et al., (1996). We considered convection, starspots and active regions, and distinguished between solar-type and evolved stars. Estimates of the visibility function, i.e., the normalized Fourier transform of the expected intensity distribution, are presented in fig. 3 for a solar-type star and in fig. 4 for a giant. The figures show the various contributions to visibility magnitude. Due to the vast range in both angular frequencies and visibility magnitude, the figures show log-log plots. In order to be independent from assumptions about the distance to the star, angular frequencies are shown in "inverse stellar radii" (this unit corresponds to one interferometer fringe across the stellar diameter). The scale in arcsec shown on the top of the plots illustrate the scales which result from placing the Sun (fig. 3) and a K giant with 25 solar radii (fig. 4) at a 10 pc distance. The contributions to the visibiltiy result from the following phenomena.

Stellar disc. Its sharp edge produces the bulk of the interferoemtric signal at low angular frequencies. Fig. 3 shows the Airy function-like visibility of a disc with a limb darkening coefficient of 0.32. The visibility at higher frequencies is indicated as the dot-dashed line with a high frequency turn-off related to the pressure scale height in the photosphere. The stellar disc component in Fig. 4 is shown for a limb darkening coefficient of 1.0.

Star spots and active regions. Both spots and plages would contribute signals to the low to medium frequency range. The visibility contribution shown in Fig. 3 represents five starspot groups, each with a diameter of 2% of the stellar diameter and a rest intensity of 0.05 times the disc center intensity. The dotted lines represent a variation of the signal by a factor of $\pm\sqrt{5}$. Spots with a diameter of 10% of the stellar diameter and a rest intensity of 40% were assumed for the evolved star. Lower spot contrasts on giants are expected due to the larger pressure scale heights and the lower magnetic field strengths.

Small-scale magnetic fields. The solar surface is dotted with magnetic field concentrated in small elements which manifest themselves as network bright points (NBPs). The contribution shown in Fig. 3 assumes a solar density of NBPs with a contrast of 1.6 and a 50 km diameter. There is no such contribution for the evolved star within the range covered by the plot in Fig. 4.

Convection. The contribution shown in Fig. 3 represents solar granulation with an *rms* contrast of 0.15 times disc central intensity and an upper cutoff frequency of 1400 km. The lower cutoff was arbitrarily set to 10 times the upper cutoff. Little is known about the properties of convection for stars of types much later than the sun. We show in Fig. 4 the range of visibility signal one would expect for an intensity contrast varying from 1% to 25% for convective cells ten times the size of solar granules, to account for the increase in size with decreasing surface gravity.

The observation of surface phenomena on late dwarfs with VLTI is next to hopeless. The disc of the Sun at 10 pc would be just barely resolved by VLTI baselines. Spots and active region on these low activity stars just produce too little variation in visibility to be measurable. Convection is only accessible to

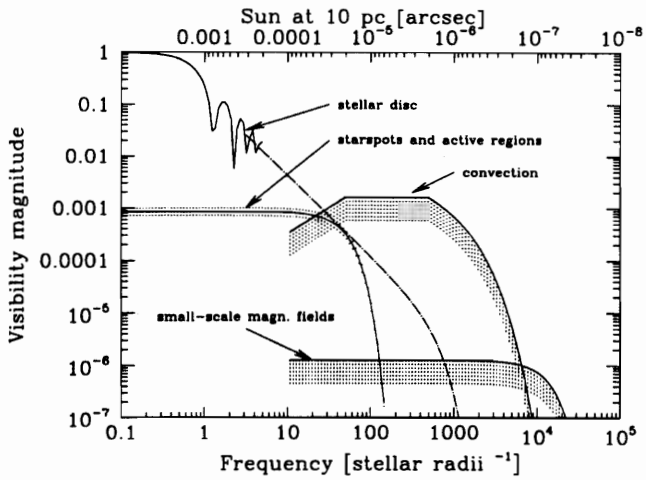

Fig. 3. Visibility magnitude for a solar type star.

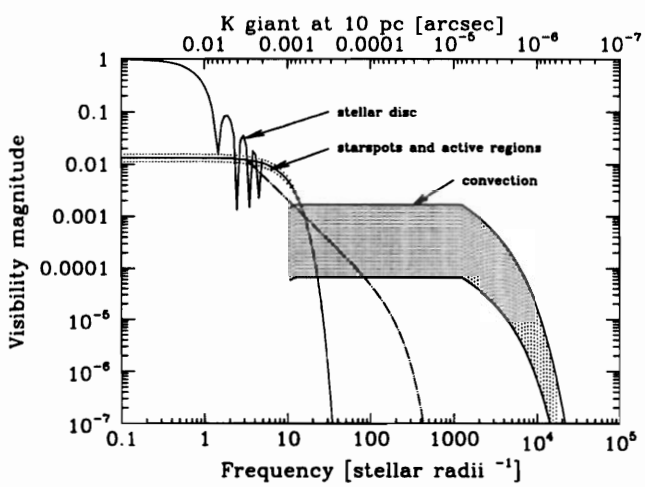

Fig. 4. Visibility magnitude for a giant star.

baselines of order of several to several tens of kilometers. The situation looks much better for active stars. Starspots and active regions of the sizes implied by Doppler imaging should be easily observable with VLTI on a number of stars. However, the stars one would observe with the VLTI are not necessarily good targets for Doppler imaging and *vice versa*.

Figs. 5 and 6 illustrates the effect of a starspot on the visibility function. Fig. 5 shows a contour plot of the surface intensity distribution, with some center-to-

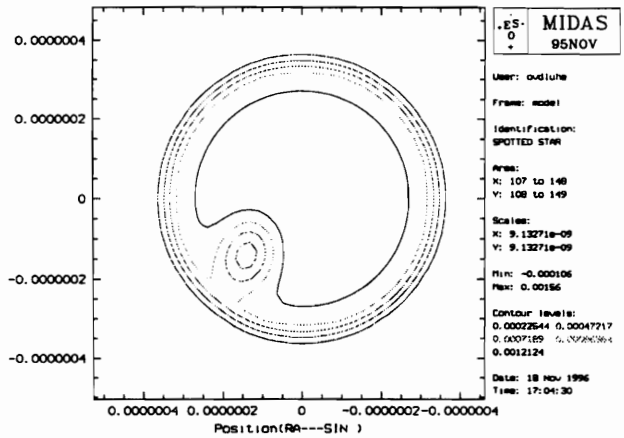

Fig. 5. Intensity distribution of a star with a spot.

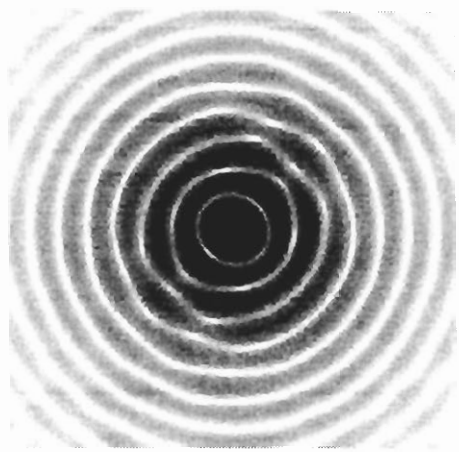

Fig. 6. Visibility magnitude of the spotted star.

limb variation and a dark spot off the center near the lower left limb. Fig. 6 shows the resulting visibiltiy magnitude in a logarithmic scale over three decades. The most prominent feature is the maximum near the origin at the center and the rings, those represent the sharp stellar limb. The spot does not manifest itself by adding a signal to the visibility function, but rather by distorting the shape of the rings. This is the signature which must be detected by the interferometer in order to reconstruct images with starspots.

4 Simulations of Observations with VLTI

We have performed simulations of observations of stellar surfaces using the CalTech VLBI data reduction package (Pearson, 1991). An example is shown in figures 7 and 8. The simulated configuration of the VLTI included the four large 8m telescopes and three 1.8m Auxiliary telescopes at locations where they optimally match the configuration of the large telescopes in order to achieve a compact, well covered UV plane. The resulting synthesis coverage using the Earth's rotation for a source at $-65°$ declination is shown in fig. 7. The same configuration was used to simulate observations of the star model shown in fig. 5 at declinations of $+15°$, $0°$, $-15°$, $-35°$, and $-65°$, thus covering the range of declinations which are relevant to the VLT. The zenith distance was always limited to $60°$.

The simulated star has an apparent diameter of 5 mas and a flux of 0.9 Jy ($m_R = 8.89$). The observing wavelength is Hα (6563 Å). Simulated visibility and closure phase data were subjected to Fourier inversion which yields a dirty map. Several thousand iterations of CLEAN were used to obtain clean maps of the stellar surface. A rendition of the model source at infinitely good resolution (top) and the CLEANed maps are shown in fig. 8. This simulation is best suited to assess the aperture synthesis capability of various configurations of the VLTI when using standard radio interferometry data analysis procedures, rather than to assess sensitivity issues.

The CLEANed maps always show the spot at its correct position near the lower left limb. The maps for declinations near the celestial equator appear mottled, while the maps for $-35°$ and $-65°$ seem to represent more faithfully the stellar surface at the resolution which can be obtained with the array. The reason is that the UV coverage near the equator is always worse than the one for southern declinations. The inversion procedure used here is easy to implement in the given context, but is not the best suited for an extended source like a stellar surface. CLEAN attempts to fit point sources to a dirty map, and a stellar surface is not very well represented by that process, which explains the somewhat lumpy reconstructed maps. A model fitting procedure, with initial model parameters taken from the CLEANed maps, may have produced better results, but this was not done here. All in all, one can conclude that the VLTI will be able to produce maps of stellar surface in Hα with a quality which would allow one to study large starspots on the sample of stars whose apparent diameters exceed some 3 mas.

5 Sensitivity

There are two factors which limit the sensitivity of the VLTI to map surfaces of stars. First, in order to obtain necessary spectral diagnostics, the spectral resolution must be rather high, of order 50000. The flux per spectral channel is therefore rather low, which requires integration times that exceed the atmospheric correlation time scales. Active fringe tracking guarantees long coherent

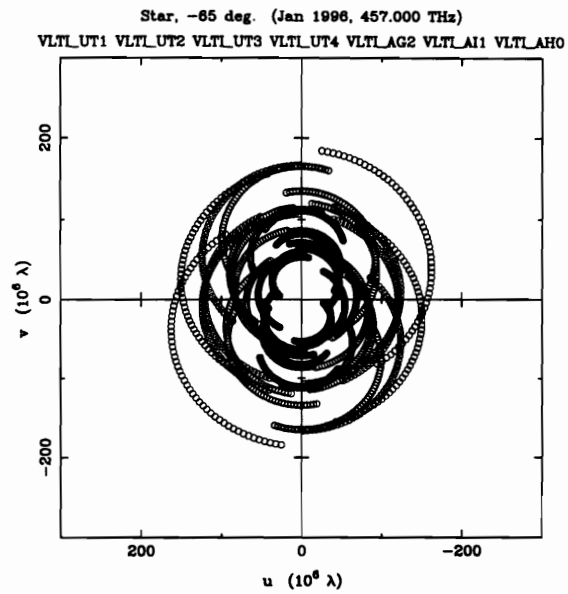

Fig. 7. Fourier domain (UV) coverage of the simulated observations for a source declination of -65 degrees.

integration times of fringes in narrow spectral bands. The fringe tracker sensor can be used with broad spectral bands, but requires integration times shorter than the atmospheric correlation time. The sensitivity of the fringe tracker therefore determines the limiting magnitude and must be used on shorter baselines for which the intrinsic visibility of the source is high. For an array with N elements, fringe tracking must be performed on at least $N-1$ baselines, but the fringe signal will be stabilized on all $N/2(N-1)$ baselines. A proper selection of the baseines used for finge tracking is therefore necessary in order to maximise the sensitivity.

The second factor is the low visibility of the source. Figs. 3, 4 and 6 demonstrate that the intrinsic visibility of the phenomena of interest is of order $10^{-2} \cdots 10^{-3}$ which is rather low. The visibility determines directly the signal to noise ratio. The detection of intrinsic visibilities of 10^{-2} is nowadays demonstrated, some further development for detecting 10^{-3} will be necessary.

The sensitivity of an optical interferometer depends on several factors. If the beam combiner rejects all photons which are scattered by atmospheric and instrumental aberrations by, e. g., using an Airy-disc sized mode stop in an image conjugate just before beam combination, the signal to noise ratio SNR of a photon and detector noise limited visibility measurement is given with

$$\mathrm{SNR} = \frac{SN_p}{\sqrt{1 + SN_p + N_d^2}} \frac{V}{N_{Tel}} \sqrt{K} \ . \tag{1}$$

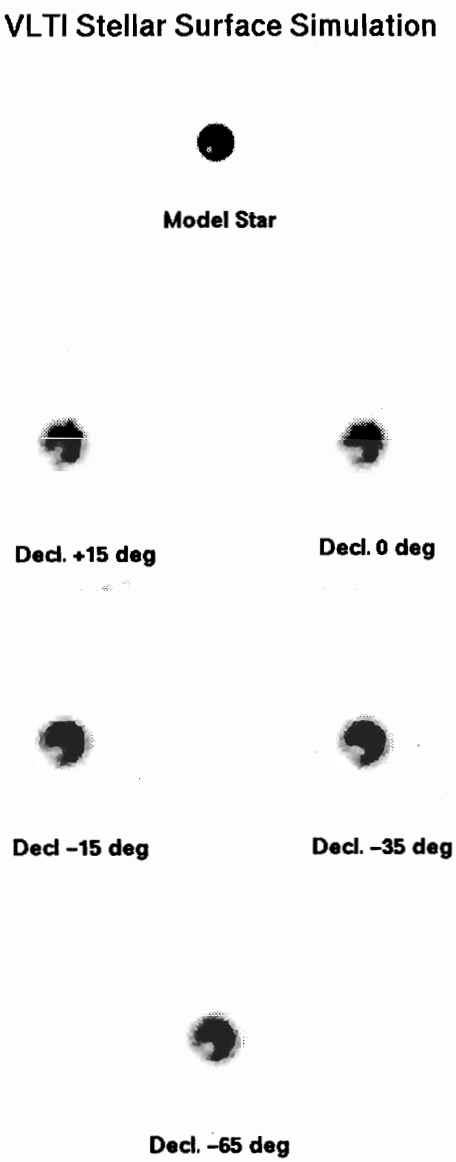

Fig. 8. Sample CLEAN maps of a stellar surface at various declinations.

N_p is the number of photons collected by all telescopes, including losses due to atmosphere, transmission of optics, and detector response. S represents the Strehl ratio of the optical train, including atmosphere effects and any compensation by adaptive optics, at the point of beam combination. The product SN_p is the number of detected *coherent* photons – these are the photons which contribute to the visibility signal. Because of the mode stop the number of photons which contribute to the noise is also SN_p. N_d is the number of photons which are equivalent to the *rms* detector readout noise. V is the intrinsic visibility of the source at the observed baseline. N_{Tel} is the number of elements in the array. K is the number of *incoherently* averaged visibility measurements. The latter comes about when the interferometer operates in open loop geometric delay tracking mode, which makes it necessary to average the visibility modulus of many short exposures.

Figs. 9 and 10 show the visibility amplitude signal–to–noise ratio for a single baseline VLTI with two 8m Unit telescopes and with two 1.8m Auxiliary telescopes in the Johnson H band. Each curve within a plot represents a different intrinsic visibilitiy of the source, ranging from 1 to 10^{-3}. Each plot within a set represents a different fringe integration mode. The top left curves represent the SNR for short integration times needed for fringe tracking using the entire H band. The top right curve applies to long on-detector integration times (900 s) but with a narrow spectral band of $0.2\mathring{A}$ and represents the SNR in a single high resolution spectroscopic channel. The bottom two sets of curves apply to incoherent averaging of short exposures at medium passbands ($100\mathring{A}$), the left with adaptive optics, the right without.

An adaptive optics system which improves the Strehl ratio at each telescope to about $0.4 \cdots 0.5$ in the H band was considered. This applies to all except to the bottom right plots, where the Strehl ratio is determined by atmospheric conditions (Fried parameter $r_{o,H}$ = 75cm which results in $S = 0.009$ for 8m telescopes and $S = 0.17$ for 1.8m telescopes). Also, the term SN_p in the square root in the denominator of eqn. 1 was replaced by N_p in the bottom right plots because a mode stop would make little sense in a seeing limited configuration. The short exposures are determined by the atmospheric correlation timescale. With a turbulence weighted mean wind speed of $5ms^{-1}$, the resulting short exposures amount to 0.023s for the plots shown here. The overall throughput including detector sensitivity was set to 0.1 for the two top plots, and to 0.05 for the plots at the bottom. This was to account for solid state detectors in the first two cases, which include detector readout noise equivalent to a NEP of $10^{-16}W/\sqrt{Hz}$. For the bottom two curves, photon counting detectors with zero readout noise were assumed.

Most curves exhibit a bend which separates two regimes. For fainter sources, the detector noise dominates and the SNR is proportional to the signal, whereas for bright sources, photon noise dominates and the SNR grows with the square root of the signal. Fringe tracking is possible with the 8m telescopes for sources with $m_H \leq 15$ provided the intrinsic visibiity is high. Stars with $m_H \leq 10$ can be fringe tracked on baselines with intrinsic visibilities as low as 0.02. The

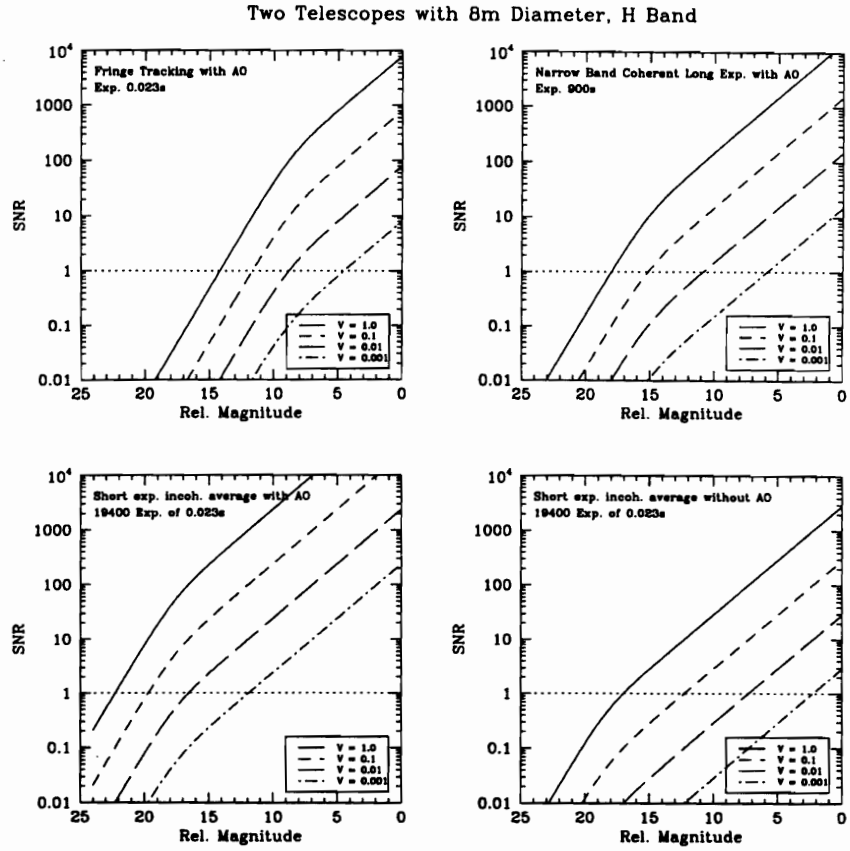

Fig. 9. Signal to noise ratio of two 8m telescopes in the H band. See text.

long exposure integrations can go considerably fainter, it should be possible to detect visibilities between 210^{-2} to 10^{-3} for the magnitude range from 12 to 6. The 1.8m Auxiliary telescopes are considerably less sensitive for the fringe tracking and long integration modes with adaptive optics, which is what one would expect. The magnitude range does not go much fainter than $m_H = 8$. The incoherent modes which require less real time control can go faint only when adaptive optics are used with the 8m telescopes. A totally passive mode (no adaptive optics and no fringe tracking) would be best done using only the 1.8m Auxiliaty telescopes.

The conclusion of this analysis is that the sensitivity of the VLTI is well matched to the problems one can expect. Faint sources are likely to be less resolved than bright ones implying higher intrinsic visibilities and thus more signal. Stars with m_H fainter than 10 have apparent diameters less than 5 mas,

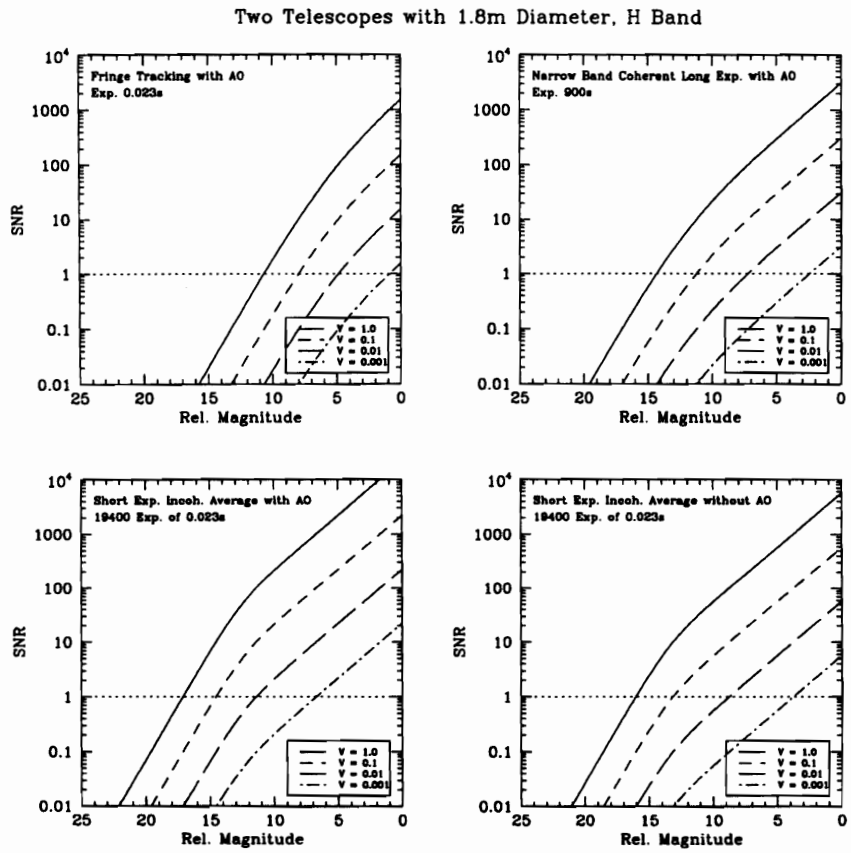

Fig. 10. Signal to noise ratio of two 1.8m telescopes in the H band. See text.

and will require measurements of visibilities of order 10^{-2}. This can be relatively easily achieved with the 8m telescopes. Obviously, well resolved stars tend to be rather bright, and an intrinsic visibility of order 10^{-3} should be easier to detect. The fringe tracking mode appears to be more demanding in terms of sensitivity compared to observations with narrow spectral bands in conjunction with long exposures.

6 Conclusions

Interferometry with the VLT will produce crucial new insight in the understanding of stellar atmospheres by providing direct images of stellar surfaces. By assessing the potential of VLTI we conclude that about 2000 stars will be resolved to VLTI baselines and that it should be possible to obtain maps with

useful detail for some 400 stars. A large fraction of the latter are late type giants, which indicates that at least for this class of stars, a fairly complete sample of maps should be doable. We expect that the available baseline length will limit the resolution to structures of the order of large spots and active regions on magnetically active stars.

We use computer simulations to study in detail the performance of VLTI, to investigate operational requirements of a given science program, and to study data analysis methods. Standard VLBI data reduction techniques will be sufficient for broadband imaging, but more sophisticated analysis and model fitting may be necessary for high resolution spectroscopy. It will also be necessary to include many baselines into the array if detailed maps of the stellar surface are to be made.

A sensitivity analysis shows that Auxiliary telescopes suffice for observing the brighter stars and / or with baselines at which the visibiity of the source is high. This is mainly due to sensitivity limitations of the fringe tracking mode. Unit telescopes will become necessary to measure fainter stars with magnitudes between 10 to 15 and with high spectral resolution. The operation of Unit telescopes at near infra-red wavelengths will require adaptive optics.

References

Fracassini, M., Pasinetti-Fracassini L. E., Pastori, L., Prioni, R. 1988, *Bull. CDS* 35, 121.

von der Lühe, O., Schüssler, M., Solanki, S., Caligari, P. 1995, *Science with the VLT*, J. R. Walsh and I. J. Danziger (eds), ESO Astrophysics Symposia, Springer, p. 94.

von der Lühe, O., Solanki, S., Reinheimer, Th. 1996, *Stellar Surface Structure*, K. Strassmeier and J. Linsky, (eds), IAU Coll. 176, pp. 147–163.

Pearson, T. J. 1991, "Introduction to the CalTech VLBI Programs," California Institute of Technology VLB Manual.